American Journal of Fluid Dynamics 2014, 4(2): 56-68
DOI: 10.5923/j.ajfd.20140402.02

Experimental and CFD Analysis of Non-Newtonian Pseudoplastic Liquid Flow through Vertical Helical Coil

Tarun Kanti Bandyopadhyay[1,*], Sudhansu Sandhibigraha[2], Sudip Kumar Das[3]

[1]Department of Chemical Engineering, NIT, Agartala, Tripura (W), Jirania, 799055, India
[2]Department of Hydroinformatics Engineering, NIT, Agartala, Tripura (W), Jirania, 799055 India
[3]Department of Chemical Engineering, University of Calcutta, 92, A.P.C. Road, Kolkata – 700009, India

Abstract Experimental studies on the pressure drop in vertical helical coils using non-Newtonian pseudoplastic liquid have been reported. The effects of different variables such as liquid flow rate, coil diameter, pseudoplasticity of the liquid on the frictional pressure drop have been investigated. The Computational Fluid Dynamics (CFD) analysis using Fluent 6.3 software evaluates the static pressure at hexahedral and tetrahedral grid, total pressure and velocity magnitude at the different angular plane of the vertical helical coils. The CFD results compare with the experimental data. CFD analysis also gives the details inside flow phenomena of the coil.

Keywords Vertical Helical Coils, Pressure drop, Non-Newtonian Pseudoplastic, CFD, Fluent 6.3 Software SCMC

1. Introduction

Helical coils are extensively used in compact heat exchangers, heat exchanger networks, heating or cooling coils in piping systems, intake in air crafts, fluid amplifiers, coil steam generators, refrigerators, nuclear reactors, thermos phones, other heat-transfer equipment and chemical plants, as well as in the food and drug industries. But non-Newtonian fluid flows through helical coils are mainly used in pulp and paper, paints, tooth-paste industries. One of the main advantages in the use of helical coiled tubes as chemical reactors or heat exchangers lies in the fact that considerable lengths of tubing can be contained in a space-saving configuration that can easily be placed in a temperature-controlled environment. The heat and mass transfer coefficients in helical coiled tubes are higher than those in straight tubes. When fluid flows through a curved pipe, the presence of curvature generates a centrifugal force that acts at right angles to the main flow, resulting in secondary flow. The strength of the secondary flow depends on the curvature of the surface. A literature survey indicates that numerous studies dealing with flow phenomena and pressure drop in single-phase flow through helical coils have been published. These are well summarized in Berger et al. [1], Shah and Joshi [2] and Das [3]. Coiled tubes are basically Dean-vortex-based systems, in which the curvature directly induces secondary flows to enhance the radial mixing. The formation of centrifugal instabilities in the flow creates higher vortices and also shear rates at the wall of the coil thus stronger mixing effect generates than the normal Taylor vortices Tiwari et al. [4] and Gelfgat et al. [5]. The use of Dean Vortices were utilized in the various Membrane module configuration. U-bend and helical tubes are the most commonly used geometries So et al. [6], Chung et al. [7], Yamamoto et al. [8], Moulin et al. [9]. Moulin et al. studied the wall shear stress by using four types of tube geometry, i.e., straight, torus, helical and woven, and concluded that the helical geometry gives more wall shear stress. Guan and Martonen [10] simulated by using CFD to observed the developing length of velocity patterns and transitional character of fluid flowing in curved geometry.

In order to achieve optimum performance, an accurate design technique (computational fluid dynamics technique with the help of FLUENT 6.3) is necessary to predict the single–phase pressure drop through vertical helical coil tube.

Table 1. Range of variables investigated

Variables	Range
Liquid flow rate, m^3/s	$3.334 – 15.003 \times 10^{-5}$
Concentration of SCMC Solution (kg/m^3)	0.2 - 0.8
Flow behavior index of the liquid	$0.6015 \le n' \le 0.9013$
Consistency index ($Ns^{n'}/m^2$) of the liquid	$0.0142 \le K' \le 0.7112$
Density of the liquid (kg/m^3)	$1001.69 \le \rho \le 1003.83$
Tube diameter, mm	9.33 – 12.00
Coil diameter, m	1.762 – 2.667
Number of turns	6 - 10

* Corresponding author:
banerjeetarun@yahoo.com (Tarun Kanti Bandyopadhyay)
Published online at http://journal.sapub.org/ajfd

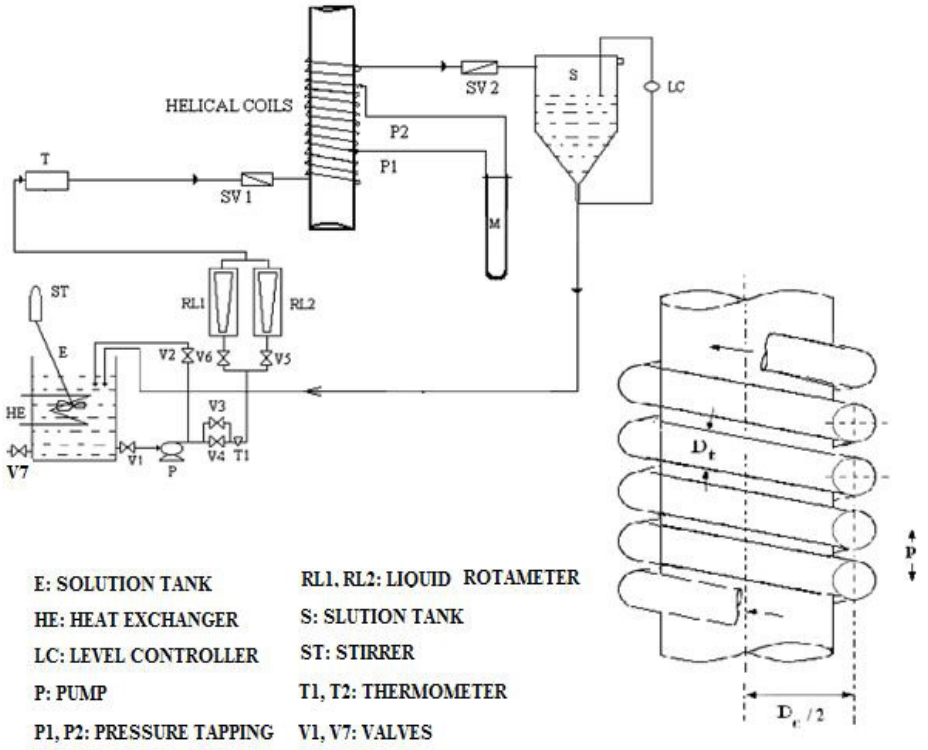

E: Solution Tank, HE: Heat Exchanger, LC: Level Controller, P: Pump, P1, P2: Pressure Tapping, RL1, RL2: Liquid Rotameter, S: Level tank, ST: Stirrer, T1, T2: Thermometer, V1-V7: Valve

Figure 1. Schematic diagram of helical coil

2. Experimental Procedures

The schematic diagram is shown in the Figure 1 and the dimension and flow characteristics in Table 1.

The experimental apparatus consisted of a solution tank, heat exchanger, centrifugal pumps, a test section, control and measuring systems for flow rate, pressure drop and other accessories.

The liquid storage tank was a cylindrical vessel of 0.45 m^3 capacity and was fitted with a propeller type of stirrer for uniform mixing of sodium salt of carboxymethyl cellulose (SCMC) solutions. The test liquids were prepared by dissolving the required amount of SCMC in tap water, stirring until a homogeneous solution was obtained and kept around 15hr. for aging. Adding trace amounts of formalin prevented biological degradation. Content of the tank was kept at a constant temperature by circulating water through a copper coil.

Thick walled flexible, transparent PVC pipes with internal diameter of 0.00933 – 0.01200 m having the total length of the tube as 15 m was used as experiment. The PVC pipes were wound round a cylindrical hard PVC frame of known diameter to form a helical coil. The helical coils were fixed and carefully tightened with clamps in order to avoid deformation of the tube. Changing the diameter of the frame and diameter of the tube will vary coil diameter. The tubes were wound in closed packed fashion so that the pitch is equal to the outer diameter of the tube and maintained constant for all cases. Helix angle of 0^0 was used for experiment. The entire test section was vertically mounted on frame to prohibit vibration. Detailed dimensions of the coils used in the experiments are given in Table 1.

The test liquid was circulated from the tank by means of a centrifugal pump to the helical coil test section. Its flow rate was controlled by bypass valves and was measured by a set of rota meters (RL1 and RL2) [Transducers and Controls Pvt. Ltd., Hyderabad, India, Accuracy ±2%] connected in parallel. The liquid was discharged in the level control tank and was returned to the liquid storage tank.

The level control tank diameter 0.25 m and height 0.6 m was made from mild steel sheet. The liquid level in the level control tank was always kept below the test section. The level of liquid in the control tank was controlled with the help of a level controller.

Four aqueous solutions of SCMC (Loba Cheme Pvt. Ltd., Mumbai, India) of approximate concentrations 0.2 kg/m^3, 0.4 kg/m^3, 0.6 kg/m^3 and 0.8 kg/m^3, were used as non-Newtonian liquids. The properties of the non-Newtonian liquids were measured by standard techniques, i.e., viscosity was measured by pipeline viscometer, surface tension by Dunouy tensiometer and density was measured by specific gravity bottles. The PVC pipes were wound round a cylindrical hard PVC frame of known diameter to form a vertical helical coil. Changing the diameter of the frame and diameter of the tube will vary coil diameter. The tubes were wound in closed packed fashion so

that the pitch is equal to the outer diameter of the tube and maintained constant for all cases. Helix angle of 0° was used for experiment. The pressure taps were located at the middle of the vertical helical coils. The upstream pressure tap was mounted after 4 to 6 coil turns in order to reduce the effect of the upstream flow and downstream pressure tap also mounted before 4 to 6 coils turns to reduce the downstream flow. The two pressure tap were adjusted to ensure that they were on the same vertical line. A simple U-tube manometer containing mercury beneath the water measured the pressure difference.

The objective of the research work is evaluating the performance of the facilities of software. CFD analysis complements testing and experimentation. It reduces the total effort required in the experiment design and data acquisition. It offers low cost than the physical testing methods which help in understanding essential engineering data for design which can be expensive. Fluent 6.3 solvers are able to solve the details flow structure, flow phenomena, static and total pressure, pressure drop inside the vertical helical coil. The simulated data is validated with experimental data. It can help the design of a vertical helical coil. This is helpful to solve the many industries problem say, paper pulp, paints flow, starch flow, rubber flow for helical type coil pipe and food flow in Stomach, blood flow in different types of veins, arteries.

3. CFD Analysis

3.1. Mathematical Model

The present work considers a coiled tube with circular cross-sectional diameter, d, coiled diameter D_c, pitch is equal to outer diameter of pipe and curvature ratio = D_c/d. The axis of the coil is vertical Figure 2. The cartesian coordinate system was used to represent (X, Y, Z) a coiled tube in the numerical simulation Fig. 3. Dilute solution of SCMC follows the laminar non-Newtonian pseudo plastic Power law model.

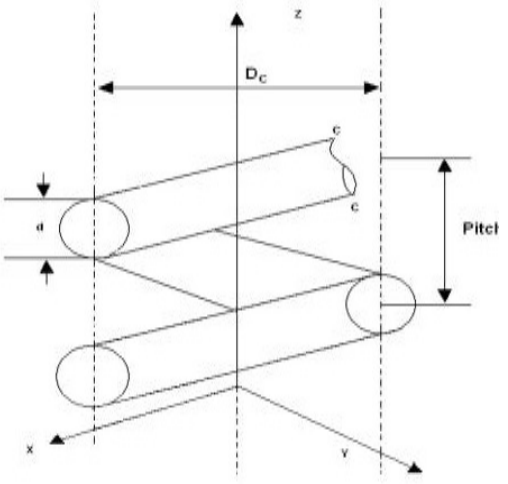

Figure 2. Schematic geometry of the coil

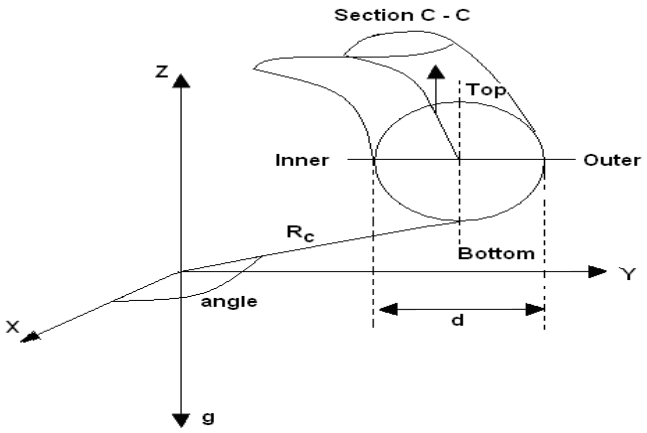

Figure 3. Co-ordinates of the coiled tube

3.2. Governing Equations and Numerical Methods

3.2.1. Model Development

The numerical model considered assumes that flow through the tube is laminar, axisymmetric, incompressible, isothermal and fully developed. Fully developed flow length (entrance length) is used here to keep the cost down. Computer memory will be used low during the time of grid generation, simulation and hence lowering the convergence time. The fact that the flow was laminar was confirmed by the helical coil pipe Reynolds number < 2100. At higher Reynolds number greater the value of entrance length and hence CFD simulation computationally expensive.

The flow of non-Newtonian pseudo plastic fluid (SCMC solution) inside a vertical helical coil is very complex in that it is governed by conservation of mass and momentum in the laminar flow condition. So k-ε model is not used here.

Therefore, the following assumptions were made in developing a theoretical model describing the flow through the vertical helical coil:

(i) Fluid flow in the vertical helical coil is 3-D and steady.

(ii) Fluid is incompressible and isothermal non-Newtonian fluid.

(iii) The model is limited to the flow model without considering the heat transfer, as the liquid solution temperature is constant at 32℃.

(iv) The model follows the single phase non-Newtonian power law model.

In general for non-Newtonian liquids the effective viscosity is used for calculation and defined as,

$$\mu_{eff} = K^{/}\left(\frac{8u}{d}\right)^{n^{/}-1} \tag{1}$$

The equations governing the flow are the continuity equation

$$\nabla u = 0 \tag{2}$$

Where u is the fluid velocity; and the momentum equation

$$\rho\frac{Du}{Dt} = \rho\frac{\partial u}{\partial t} + \rho u.\nabla u = -\nabla P - [\nabla\tau] + \rho g$$
$$= \mu\nabla^2 u - \nabla P + \rho g \quad (3)$$

$$\rho\frac{Du}{Dt} = \rho\frac{\partial u}{\partial t} + \rho u.\nabla u = -\nabla P - [\nabla\tau_{eff}] + \rho g$$
$$= \mu_{eff}\nabla^2 u - \nabla P + \rho g \quad (4)$$

Where ρ is fluid density, t is time, P is fluid pressure, τ is shear stress, and g is the gravitational acceleration. This can also be rewritten as

$$\tau_{xy} = K\left(\frac{\partial u}{\partial y}\right)^{n-1}\frac{\partial u}{\partial y} = \mu_{eff}\,\dot{\gamma} \quad (5)$$

$$\rho\frac{Du}{Dt} = \rho\frac{\partial u}{\partial t} + \rho u.\nabla u = -\nabla P - [\nabla\mu_{eff}\dot{\gamma}] + \rho g$$
$$= \mu_{eff}\nabla^2 u - \nabla P + \rho g \quad (6)$$

Where,

$$\nabla = i\frac{\partial}{\partial x} + j\frac{\partial}{\partial y} + k\frac{\partial}{\partial z} \quad (7)$$

Where $\dot{\gamma}$ shear rate, and μ_{eff} is the fluid apparent viscosity (effective viscosity) function. The term on the left hand side of the equation represents the mass per unit volume multiplied by acceleration; the first term on the right hand side is the pressure force per unit volume, the second is the viscous force per unit volume, and the third is the gravitational force per unit volume.

3.2.2. Non-Newtonian Fluid Model

The relationship between stress and strain for Newtonians fluids are linear and constant viscosity as a proportionality factor. But for non-Newtonian fluids this linear relation is not valid. The form of the constitutive relationship becomes material dependent.

The above equations are valid for a generalized Newtonian fluid model, where the viscosity is a function of shear rate. For the rheological models studied here, the effective viscosity function for a time-independent fluid takes the following different forms:

(i) Newtonian fluid:

$$\mu_{eff} = \mu \quad (8)$$

Where μ is the constant Newtonian fluid viscosity.

(ii) Power law fluid:

$$\mu_{eff} = K\dot{\gamma}^{n-1} \quad (9)$$

Where K is the flow consistency index and n is the flow behavior index; n < 1 for a shear-thinning fluid (pseudo plastic fluid), n > 1 for a shear-thickening fluid (dilatants fluid), and n = 1 for a Newtonian fluid.

(iii) Viscoplastic fluid:

(a) Bingham plastic fluid:

$$\mu_{eff} = \infty \text{ for } \tau \le \tau_0; \text{ and}$$
$$\mu_{eff} = \mu_0 + \frac{\tau_0}{\dot{\gamma}} \text{ for } \tau \ge \tau_0 \quad (10)$$

Where τ_0 the apparent yield stress and μ_0 is the so-called plastic viscosity;

(b) Generalized power law or Herschel–Buckley fluid:

$$\mu_{eff} = \infty \text{ for } \tau \le \tau_0; \text{ and}$$
$$\mu_{eff} = \frac{\tau_0}{\dot{\gamma}} + K\dot{\gamma}^{n-1} \text{ for } \tau \ge \tau_0 \quad (11)$$

Since the fluid is pseudo plastic non-Newtonian fluid, so model follows the power law i.e. eq (1) and (9), although both are same equation.

3.2.3. Reason for Introduction of Effective Viscosity in (eq 1)

The μ_{eff} is mainly used to know the non-Newtonian fluid properties of the fluid. This explains the Rheological properties of SCMC solutions. The SCMC solution is a time independent pseudo plastic fluid and the Oswald de-waele model or the power-law model describes its rheological behavior as,

$$T = K(-du/dr)^n \quad (12)$$

Where, K and n are the constants for the particular fluid with n < 1. The constant K is known as the consistency index of the fluid and the higher the value of K the more viscous is the fluid. The constant n is called the flow behavior index and is a measure of the degree of departure from the Newtonian behavior. For a non-Newtonian fluid with a power law model it can be show that,

$$\tau_w = D\Delta P/4L = K'(8u_l/D)^{n'} \quad (13)$$

Where, $(8u_l/D)$ is the shear rate and K' and n' are related to K and of eq (12) by the relation,

$$K' = K(3n'+1/4n') \quad (14)$$

and

$$n' = n \quad (15)$$

In eq (12) it is clear that if a logarithmic plot is made between τ_w and $8u_l/D$, a linear relation will result and the slope of the line and the intercept should give the values on n' and K' respectively.

3.2.4. Pipe Flow Viscometer Used for Measurement of Effective Viscosity

A horizontal steel tube of 0.635m internal diameter was used as the pipeline viscometer with pressure tapping at a distance of 1.85m. Measurements on pressure drop were made in the fully developed flow region of non-Newtonian liquids, in the laminar flow condition. The developed flow region was ensured by providing the necessary and sufficient straight entry, i.e., more than 50 pipe diameter length of the tube. From the pressure drop and the flow rate data the values of τ_w and $8u_l/D$ were calculated for four different SCMC solutions. After plotting τ_w vs $8u_l/D$, we are getting K' from intercept and n' from slope. Putting n' and K' values in eq (1) we are getting μ_{eff} value.

Where μ_{eff} is non-Newtonian viscosity that is only considered to be a function of the shear rate.

Where K' is the consistency coefficient (Pa s^n), $8u_l/D$ is the shear rate, n' is the power-law index that determines the class of fluid (i.e., $n' < 1$ for pseudo plastics, $n' = 1$ for Newtonian fluid, and $n' > 1$ dilatant fluid).

3.2.5. Fluent Provides Four Options for Modeling Non-Newtonian Fluids

Power law
Carreau model for pseudo plastics
Cross model
Generalized power law or Herschel–Buckley model for Bingham plastics

Note that non-Newtonian power law described below which has been used in this model.

3.2.6. Modified Power Law for Non-Newtonian Viscosity According to (FLUENT 6.3)

The non-Newtonian power law model is used in this study, where the non-Newtonian viscosity is calculated as, (FLUENT 6.3 Manual):

$$\mu_{\text{eff}} = K\gamma^{\cdot n-1} e^{\frac{T_0}{T}} \quad (16)$$

FLUENT allows upper and lower limits to be placed on the power law function, yielding the following equation:

$$\mu_{\text{eff}\,min} < \mu_{\text{eff}} = K\gamma^{\cdot n-1} e^{\frac{T_0}{T}} < \mu_{\text{eff}\,max} \quad (17)$$

Where K, n, T_0 $\mu_{\text{eff}\,min}$ and $\mu_{\text{eff}\,max}$ are input parameters. K is a measure of the average viscosity of the fluid (the consistency index), n is a measure of the deviation of the fluid from Newtonian (the power law index); T_0 is the reference temperature; and $\mu_{\text{eff}\,min}$ and $\mu_{\text{eff}\,max}$ are, respectively, lower and upper limits of non Newtonian viscosity used in the power law. If the viscosity computed from power law is less than $\mu_{\text{eff}\,min}$, the value of $\mu_{\text{eff}\,min}$ will be used instead. Similarly, if the computed viscosity is greater than $\mu_{\text{eff}\,max}$, the value of $\mu_{\text{eff}\,max}$ will be used instead.

Where T is the SCMC solution temperature and T_0 is reference temperature. Since the experimental condition is room temperature i.e. T = 32℃ and T_0 = 25℃. So all three equations (1), (9) and (16) are close to equal and μ_{eff} are calculated for different values of K' and n' for non-Newtonian pseudo plastic power law fluid i.e. our experimental results given in the Table 1.

As the flow of liquid is laminar in all cases the viscous model, i.e., laminar non-Newtonian Power Law model is used for the CFD analysis.

3.3. Boundary Condition

The above equations are solved subject to the following boundary conditions,

(i) The vertical helical coils walls are assumed rigid and a no-slip condition is imposed.

The Sodium salt of carboxy methyl cellulose (SCMC) solution behaves as a non-Newtonian pseudo plastic fluid. So its viscosity has been defined according to the non-Newtonian power law model. The introduction of no slip condition on the wall meaning that the speed of the fluid relative to the boundary is zero, but at some distance from the boundary the flow speed must equal that of the fluid bulk.

(ii) At the outlet, the velocities are free but the normal and tangential stresses are constrained to be zero and the gauge pressure is set to zero.

At the inlet, a uniform velocity profile is used with a time varying forcing function representive of flow in the left portion of the coils. Since fluid flowing in the upward direction against the gravity, negative gravitational acceleration -9.8 m/s^2 is added.

3.4. CFD Procedure

Two types of mesh have been used, about the order $3x10^4$–$1.2x10^5$ unstructured tetrahedral and boundary layer hexahedral mesh (Figures 4).

The general procedure to simulate liquid flow through coils based on Gambit 6.3 and Fluent 6.3 software is outlined below,

1. Perform meshing under Gambit 6.3:
   (a) Create a computational domain at the flow region,
   (b) The grids were generated using boundary layer hexahedral and t-grid (tetrahedral) meshes,
   (c) Controlling a smooth change in the mesh size by size functions,
   (d) Specify boundary and continuum types,
   (e) Examine the mesh to ensure that the high skewness is below 0.5 for hexahedral and below 0.9 for tetrahedral meshes.
2. Import the mesh file to Fluent 6.3 and check the mesh.
3. Define a 3-D, unsteady, implicit, and pressure-based solver.
4. Activate the single phase laminar non-Newtonian power law model.
5. Define a laminar non-Newtonian power law model.
6. Enable the SCMC properties with laminar flow conditions using the text command: define/models/ viscous/ laminar. Putting the non-Newtonian fluid values: flow behaviour index, consistency index, temperature and effective viscosity values at the inlet velocity.
7. Define the operating conditions by turning on gravity and specify the operating density.
8. Solution control methodology – Under relaxation factors – 0.5 for pressure, 0.3 for momentum, and default values for the other parameters. Standard schemes – STANDARD for momentum and 1st order upwind for other variables. Pressure-velocity SIMPLE coupling used;
9. Initialize the solution – velocity; enable the plotting of residuals during the calculation, and kept the default convergence criteria, 1×10^{-5} for all residuals except for the transport equation which residual was set at 10^{-3}.

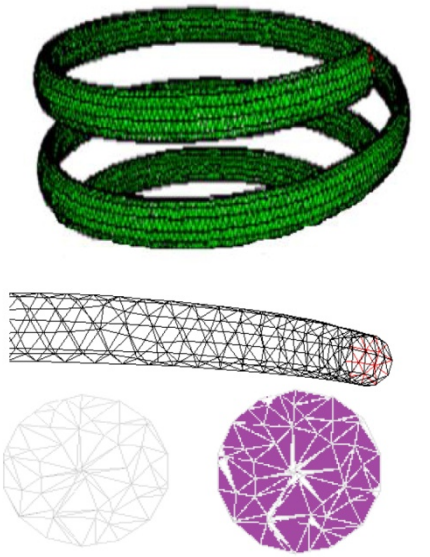

(a) Sectional view

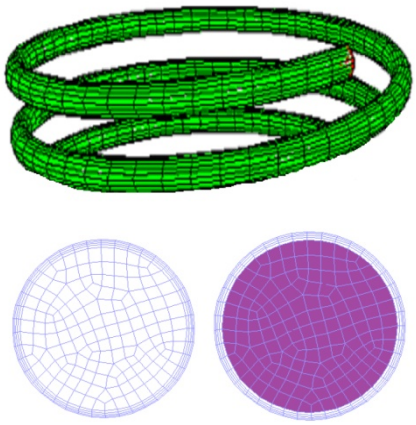

(b) Sectional view

Coil dimension D_t: 0.00933m, D_t/D_c: 0.0529, D_C: 0.2662 m, Total length: 5.01m, Turn: 6
Grid Size: Cells 108263, Faces 237397, Nodes 30060 for tetrahedral
Cells 36594, Faces 113106, Nodes 40250 for hexahedral

Figure 4. **(a)** Tetrahedral (b) Hexahedral grid

3.5. Convergence and Grid Independency

The convergence criterions were set at 10^{-5} for all equations except for the transport equation which residual was set at 10^{-3}. A computational domain L≥200D was used to ensure fully developed flow results could be obtained for all coils. In general the final results depend upon mesh geometries. Subsequent decrement and increment in mesh resolution by 50% were applied to evaluate if the employed mesh resolution was adequate to obtain accurate solutions. It was observed that when the mesh resolution was decreased by 50% the axial velocity profile was 5-10% of the currently employed mesh velocity profile for coils. As the present mesh resolution was increased by 50% the axial velocity profile changes 1-4% for coils. These results suggest that the current mesh resolution is sufficient to obtained grid independent solutions for the proposed model.

3.6. Study of Numerical Result

Table 2. No. of nodes and cells for Coarse grid

Type of grid	Coarse grid	
	No. of Nodes	No. of cells
Tetrahedral	22124	74338
Hexahedral	26542	22804

Table 3. CPU time for Coarse grid

Type of grid	Coarse grid		
	CPU time, min, RAM 4 GB	Total iteration	Time taken per iteration, sec
Tetrahedral	6	750	0.5 sec
Hexahedral	15	1880	> 2

Table 4. No. of nodes and cells for Fine grid

Type of grid	Fine grid	
	No. of Nodes	No. of cells
Tetrahedral	30060	108263
Hexahedral	40250	36594

Table 5. CPU time for Fine grid

Type of grid	Fine grid		
	CPU time, min, RAM 4 GB	Total iteration	Time taken per iteration, sec
Tetrahedral	10	650	≈ 1
Hexahedral	22	2000	< 2

Table 6. No. of nodes and cells for Finest grid

Type of grid	Finest grid	
	No. of Nodes	No. of cells
Tetrahedral	34060	112263
Hexahedral	52250	46594

Table 7. CPU time for Finest grid

Type of grid	Finest grid		
	CPU time, min, RAM 4 GB	Total iteration	Time taken per iteration, sec
Tetrahedral	18	1100	< 1
Hexahedral	30	3200	≈ 2

Table 8. Comparison of numerical vs. Theoretical values obtained for simple geometry

Variable	Exptl. Result	CFD result	% variation
u (m/s)	1.703	1.74	2.5
dP/dx (Pa/m)	2.32	2.24	3.4
u (m/s): velocity, dP/dx: Pressure drop per unit length			

Table 9. Comparison of Exptl. Result, Mishra Gupta with CFD simulated result

Variable	Mishra Gupta	Expt.	CFD result	% variation From Mishra Gupta	% variation from Expt.
Friction factor, f	0.1	0.098	0.13	3	3.2

So our CFD simulated results vary with experimental and Mishra Gupta data having range of error 2-4%.

The number of time steps was a critical issue, and its optimization required a considerable amount of computational experimentation. Also, for the solution to converge at each time step, the number of iterations per time step had to be sufficient. Whilst a large number of time steps gives better accuracy and requires a smaller number of iterations per time step to achieve convergence, it does, however, prolong the simulation considerably. The optimum number of time steps which gave an acceptable level of accuracy whilst keeping simulation time reasonable was 30 min, with 1–10 iterations per time step depending mainly on the fluid rheological properties, grid size and grid type. We observed that time taken for hexahedral grid is more comparing to tetrahedral grid. With increasing the number of grids, accuracy is more, but time needed to converge for each iteration is also more. But system is less stable. With decreasing the number of grids accuracy is less, but time taken to converge for each iteration is less. But system is more stable. When we used first order upwind scheme and under relaxation technique lowering the values of pressure and momentum value 0.3 from 0.9, getting quick convergence and stable values, but precision is not good. When we used higher order upwind scheme, then time taken for convergence is more, precision of the result is good. But system is unstable. In particular fluid with a yield stress term usually required more iteration. Convergence was assumed when mass (continuity) momentum and energy residuals reached 10^{-3} and 10^{-5} at each time step. Such a level of convergence is very high, and typically required a total of 2000 iterations. From the grid optimization technique we observed that the properties of the result are not varied with increasing the grid size. We have used here tetrahedral and hexahedral nodes 30060 and 40250. Precision of the result vary 2-4% range.

The correlation coefficient and variance of estimate are 0.8845 and 0.146 respectively. The value of t is 1.98 obtained from statistical table for 108 degrees of freedom, 0.05 probability levels and 95% confidence range.

4. Results and Discussion

Figure 4 indicates the tetrahedral grid. Figure 5 and 6 indicates the contour plot of static pressure decreases with increasing coil turn. The effect is more with increasing SCMC concentration. Figure7 indicates the **c**ontour plot of total pressure at the different angular plane and at the fixed turn1 of the coil. It indicates that the static pressure decreases with angle and coil turn. But at particular coil turn and angle fully developed flow was achieved. It is also observed that the pressure is more at the outer side wall and less at the inner wall. This is due to the action of centrifugal force. Figure 8 shows that contour plot of velocity magnitude varying with angle and coil turn. It can be seen from these figures that the maximum velocity is shifted towards the outer wall of the coiled tube. Velocity starts to change from angle 30° up to 150°. It can also depict that the flow gets almost fully developed at angle 240° to 330°. Since the velocity profiles have minor changes. As angle is increased, the axial velocity becomes asymmetrical. Due to the unbalanced centrifugal forces on the main flow, the maximum velocity is shifted towards the outer wall of the pipe. At a fixed angle and with increasing coil turn the velocity profiles have very minor changes. Secondary flow and vortices observed from the velocity profile. From Figure 9 we have observed that dynamic pressure increases with increasing concentration. This is due to centrifugal force fluid is shifted towards the outer wall. Figure 10 indicates that the frictional pressure drop per unit length of coil increases with increasing SCMC concentration. The experimental result matches well with CFD simulated result for hexahedral grid than the tetrahedral grid. Figure 11 indicates that the frictional pressure drop per unit length of coil increases with increasing coil diameter. The experimental result matches well with CFD simulated result for hexahedral grid than the tetrahedral grid. Figure 12 shows the effect of coil turn or height on the development of axial velocity profile in (a) horizontal centerline and (b) vertical centerline. It indicates that at height = 0, the velocity contours are symmetrical to the centerline of the tube. As the coil turn or height is increased the velocity contours becomes asymmetrical. Figure 13 shows that as the curvature ratio is increased, it approach towards a straight tube (curvature ratio→∞). This minimizes the curvature effect as centrifugal forces become less predominant for higher curvature ratio coils. This is evident from this figure as the velocity profiles flattens in the case of curvature ratio (D_c/d) = 18, due to action of strong centrifugal force.

Comparison with the data available in the literature

Mishra and Gupta [11] performed elaborate experiments to generate experimental data on the non-Newtonian liquid flow through helical coils. They developed empirical correlation for laminar flow as

$$\frac{f_c}{f_{sl}} = 1 - 0.033\left(\log De\right)^{4.0} \tag{5}$$

Figure 14 compared the experimental data friction factor with the Mishra and Gupta (1979) correlation and with the CFD simulated data. It is clear that the experimental data matches well with the Mishra and Gupta (1979) correlation and also the CFD simulated data. However, the hexahedral grid gives the better results than the tetrahedral grid.

5. Conclusions

1. Experiments have been carried out to evaluate the frictional pressure drop for non-Newtonian liquid flow through helical coils.

2. We have compared the experimental, Mishra Gupta data with the CFD simulated data for friction factor. From these data comparison we observed that CFD simulated data vary with our experimental data having range of 3% and Mishra Gupta 3.2%.

3. CFD analysis has been carried out for non-Newtonian liquid flow through helical coils. Commercial software Fluent 6.3, Fluent user guide, USA [13] has been used for simulation. For simulation two types of grid have been generated, i.e., tetrahedral and hexahedral grid used for simulation purpose and compare their suitability.

4. CFD analysis clearly predicts the effect of liquid concentration i.e., pseudo plasticity, effect of coil diameter on frictional pressure drop.

5. Flow phenomena inside the coils has been analyzed and observed,

(i) due to action of centrifugal force the maximum velocity shifted towards the outer wall,

(ii) maximum pressure also shifted towards the outer wall due to centrifugal action,

(iii) creation of the vortices in different location.

6. The experimental frictional pressure drop matches with the CFD analysis. However, hexahedral grid gives the better agreement.

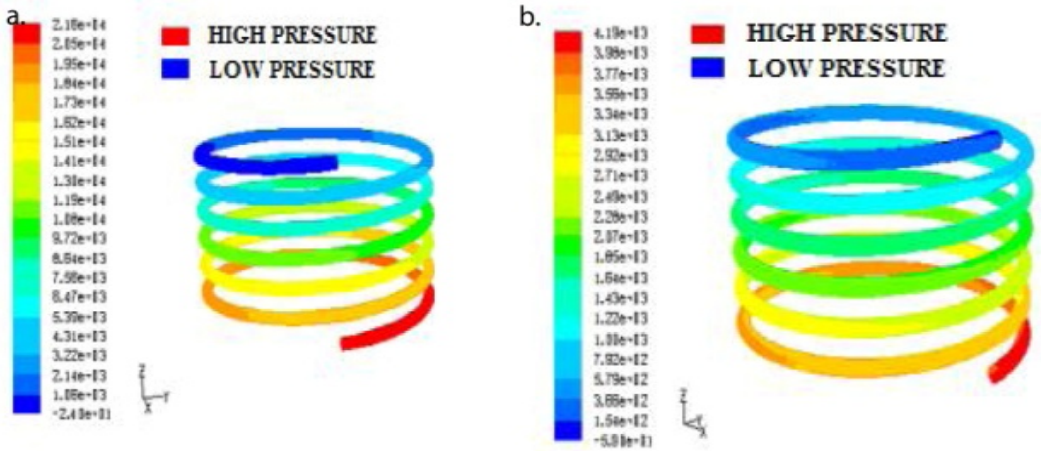

Coil dimension, D_t: 0.00933 m, D_t/D_c: 0.0529, D_C: 0.2662 m, Total length: 5.01 m, Turn: 6, Liquid velocity (m/s): 1.7086 and concentration of SCMC solution (kg/m^3): 0.8

Figure 5. Contour plot of static pressure at (a) hexahedral (b) tetrahedral grid

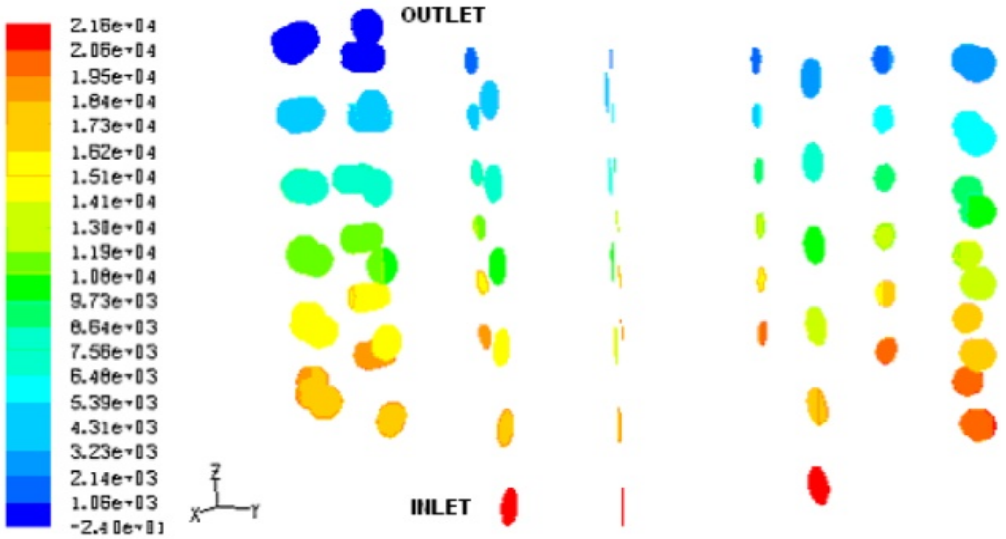

Coil dimension, D_t: 0.00933 m, D_t/D_c: 0.0529, D_C: 0.2662 m, Total length: 5.01 m, Turn: 6, Liquid velocity (m/s): 1.7086 and concentration of SCMC solution (kg/m^3): 0.8

Figure 6. Contours plot of static pressure at various planes along the length coil at hexahedral grid

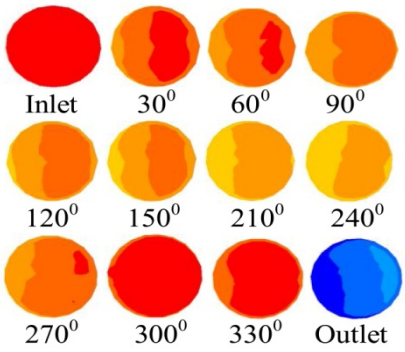

Figure 7. Contour plot of total pressure at the different angular plane and at the fixed turn1 of Coil dimension, D_t: 0.00933 m, D_t/D_c: 0.0529, D_C: 0.2662 m, Total length: 5.01 m, Turn: 6, Liquid

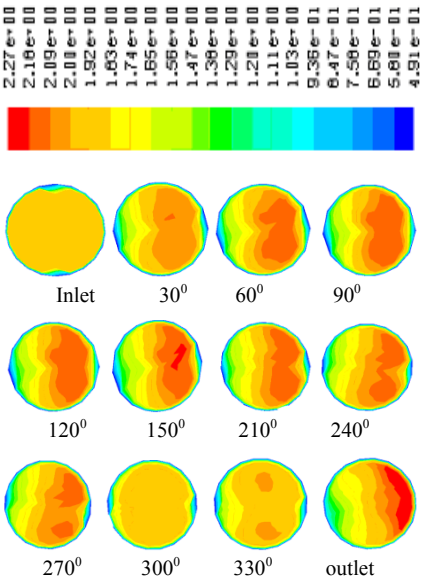

Figure 8. Contour plot of velocity magnitude at the different angular plane and at the fixed turn1 of the coil at hexahedral grid, Coil dimension, D_t: 0.00933 m, D_t/D_c: 0.0529, D_C: 0.2662 m, Total length: 5.01 m, Turn: 6, Liquid velocity (m/s): 1.7086 and concentration of SCMC solution (kg/m^3): 0.8

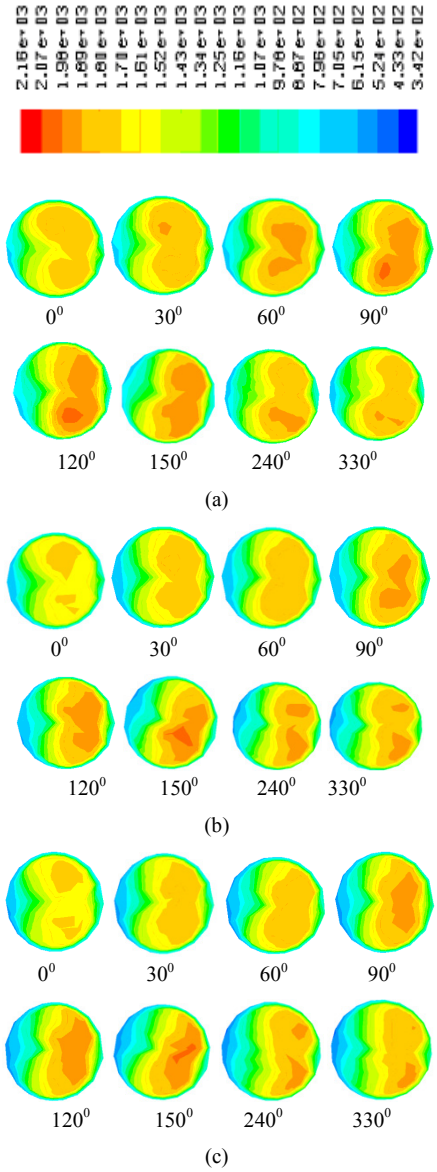

Figure 9. Dynamic pressure varying with angle for a fixed concentration, (a) 0.4 (b) 0.6 and (c) 0.8 kg/m^3, fixed turn1 of the coil

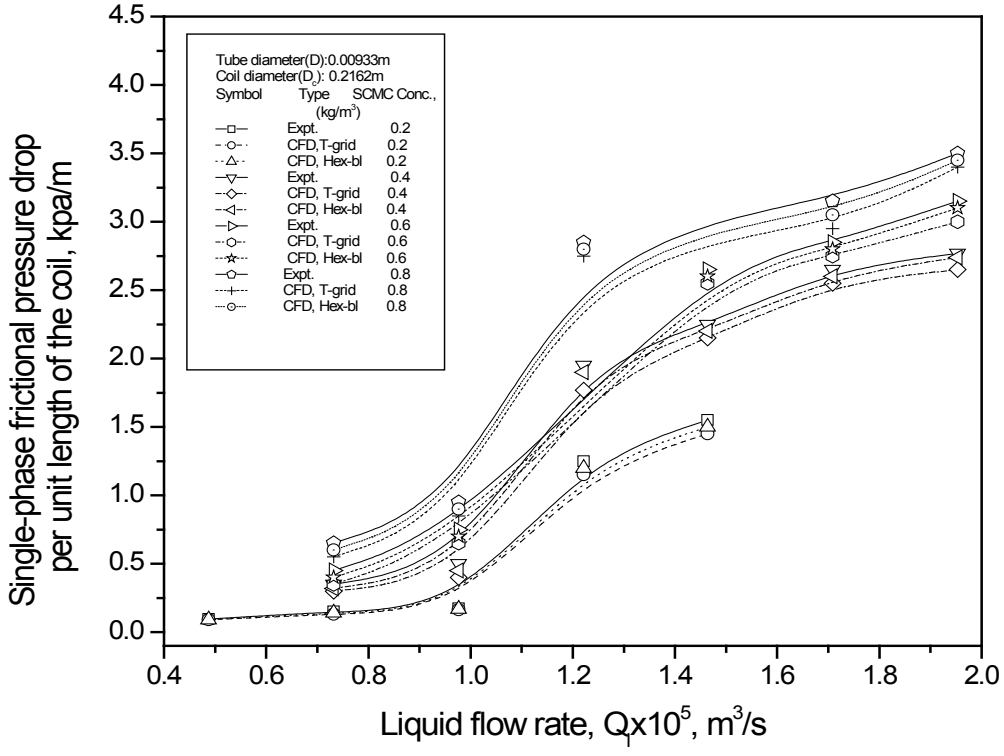

Figure 10. Comparison plot of helical coil at different SCMC concentration

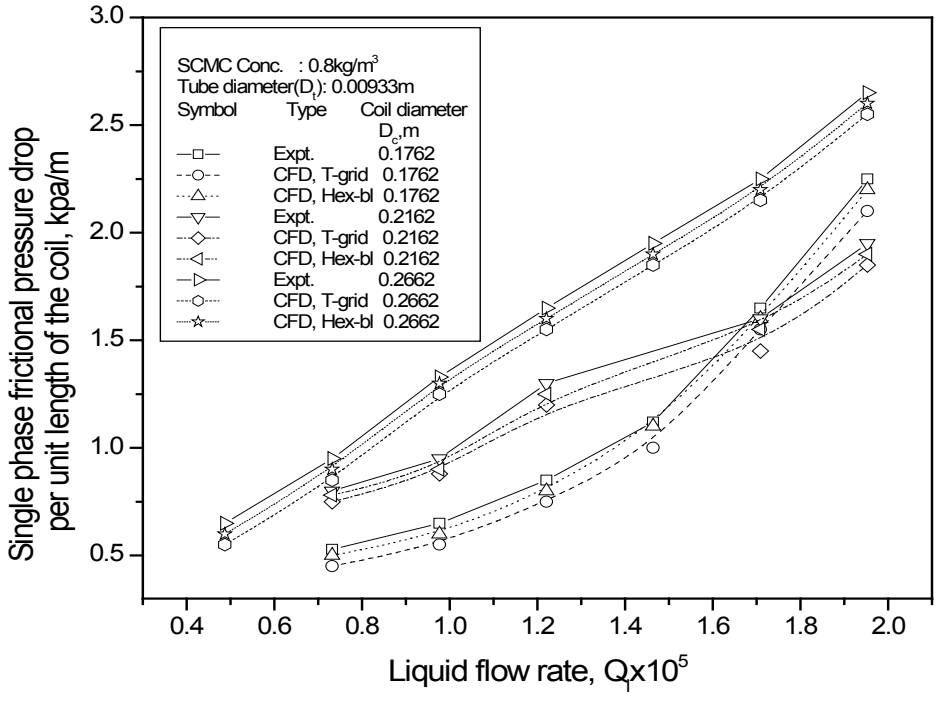

Figure 11. Comparison plot of helical coil at different coil diameter

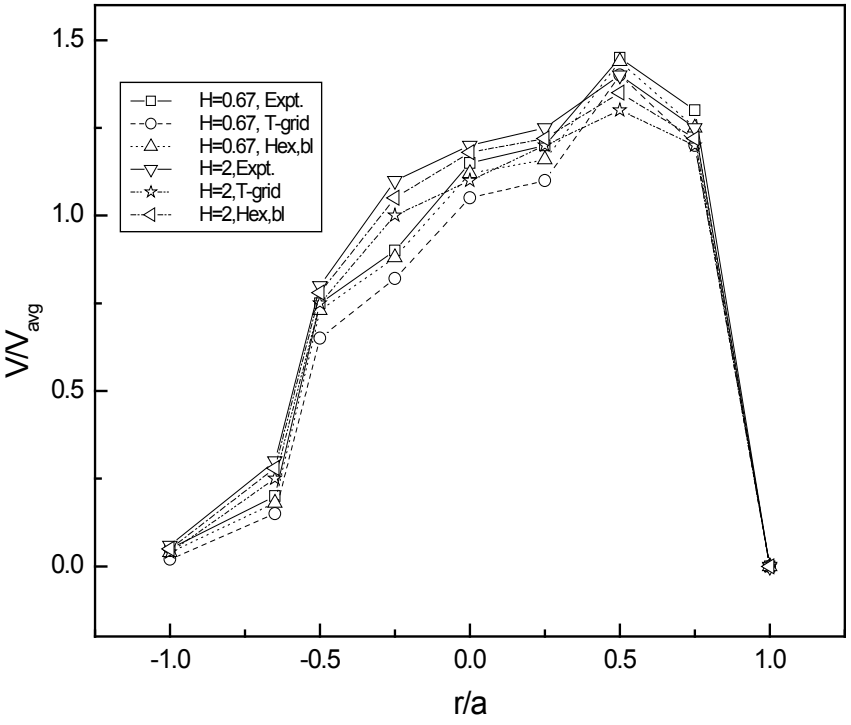

(a)

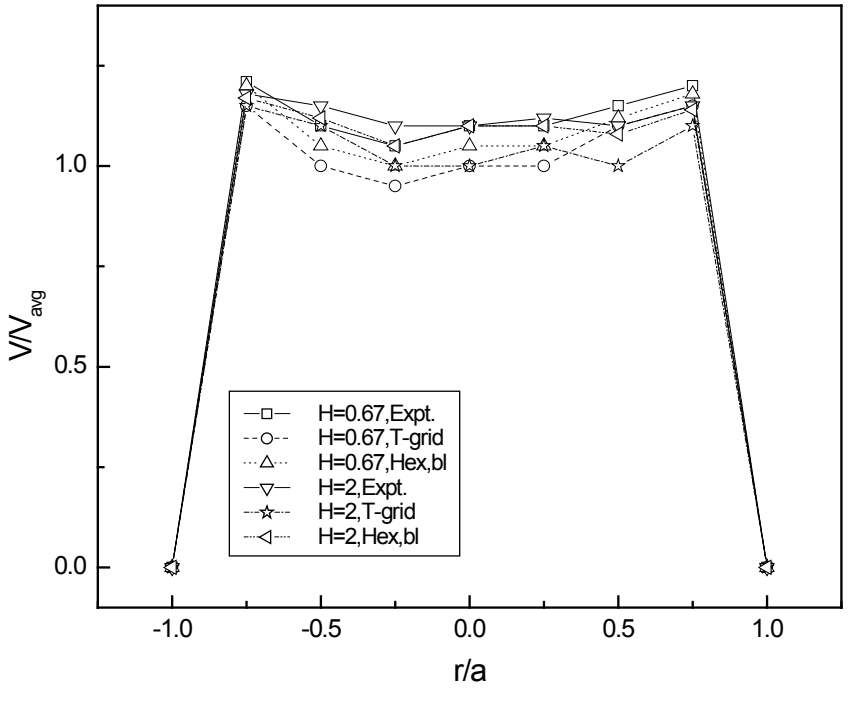

(b)

Figure 12. Effect of coil turn or coil length, H on the development of axial velocity profile in (a) horizontal centerline (b) vertical centerline

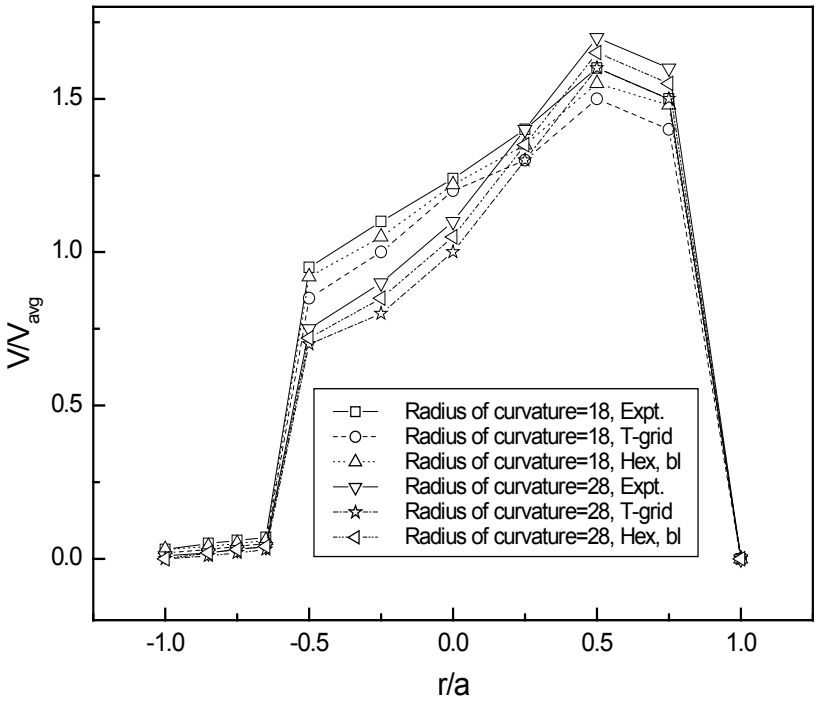

(a)

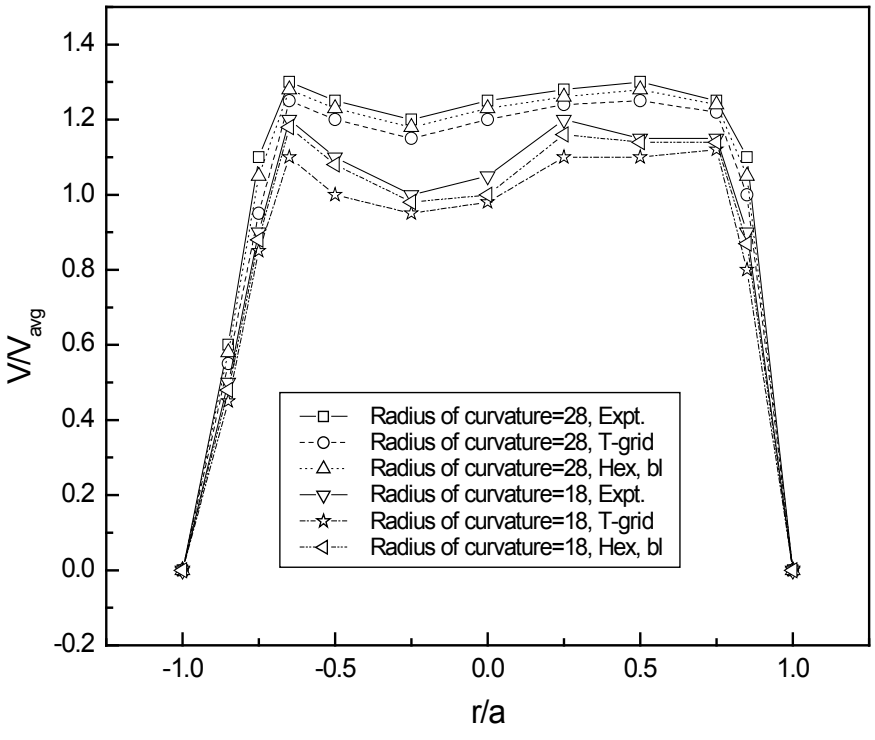

(b)

Figure 13. Effect of coil ratio on the development of axial velocity profile in (a) horizontal centerline (b) vertical centerline V_L = 1.7086 m/s, Liquid (SCMC) concentration (kg/m^3) = 0.8

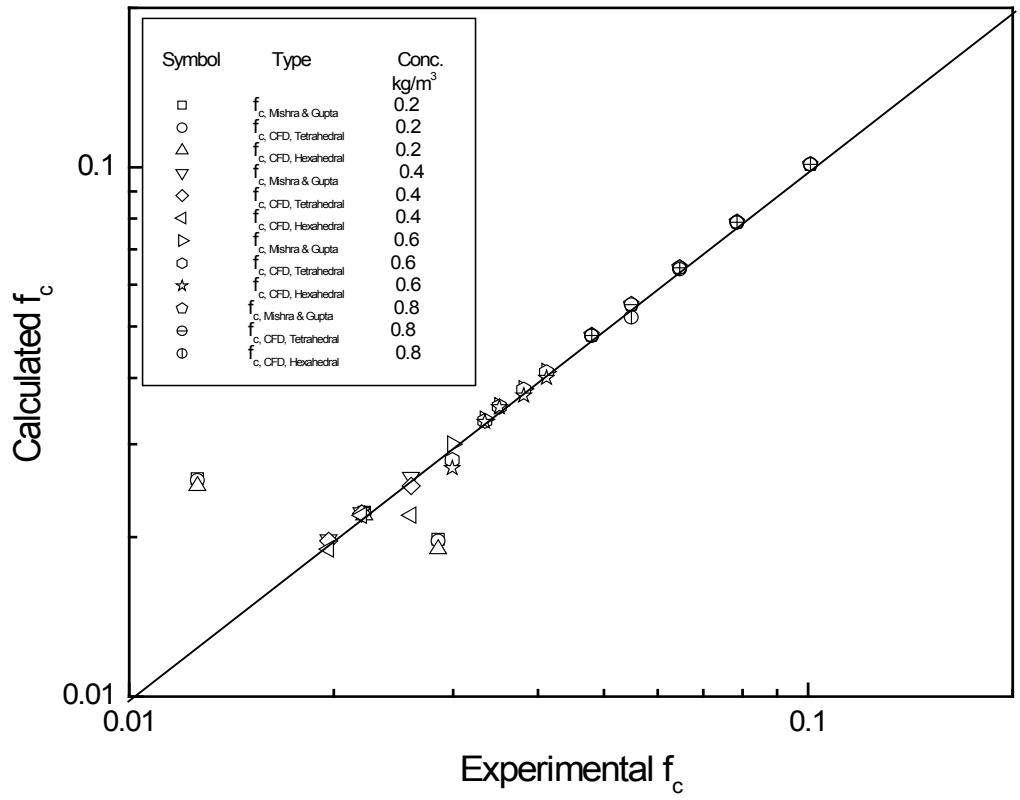

Figure 14. Comparison plot of the experimental and calculated data for friction factor across the coil for different liquid (SCMC) concentration

REFERENCES

[1] S. A. Berger, A. Talbot, and L. S. Yao, "Flow in curved pipes", *Ann. Rev. Fluid Mech*., vol. 15, pp.461-512, 1983.

[2] R. K. Shah, and S. D. Joshi, "Convective heat transfer in curved ducts", in Handbook of single-phase convective heat transfer, *Kakac, S., Shah, R. K., & Aung, W. (eds). (Wiley interscience, New York),* Chapter 3, pp. 1238, 1987.

[3] S. K. Das, "Water flow through helical coils in turbulent condition, in Multiphase Reactor and Polymerization System Hydrodynamics", N. P. Cheremisinoff Editor, Gulf Publication USA, Ch. 17, pp. 379-403, 1996.

[4] P. Tiwari, S. P. Antal, A. Burgoyne, G. Belfort, and M. Z. Podowski, "Multified computational fluid dynamics model of particulate flow in curved circular tubes", *Theor. Comput. Fluid Dyn.,* vol. 18, pp. 205-220, 2004.

[5] A. Yu. Gelfgat, A. I Yarin, and P. Z. Bar-Yoseph, "Dean vortices-induced enhancement of mass transfer through an interface separating two immiscible liquids", *Phys. Fluids,* vol. 15(2), pp. 330-347, 2003.

[6] R. M. C. So, H. S. Zhang, and Y. G. Lai, "Secondary cells and separation in developing laminar curved-pipe flows", *Theor. Comput. Fluid Dyn.,* vol.3, pp. 141-162, 1991.

[7] K. Y. Chung, M. E. Brewster, and B. Belfort, "Dean Vortices with wall flux in a curved channel membrane systems", 2 - The velocity field*, AIChE J*., vol. 42(2), pp. 347-358, 1996.

[8] K. Yamamoto, S. Yanase, and T. Yoshida, "Torsion effect on the flow in a helical pipe", *Fluid Dyn. Res.,* vol.14, pp. 259-273, 1994.

[9] Ph. Moulin, D. Veyreth, and D. F. Charbit, "Dean vortices: comparison of numerical simulation of shear stress and improvement of mass transfer in membrane processes at low permeation fluxes", *J. Membr. Sci.,* vol. 183, pp. 149-162, 2001.

[10] X. Guan, and T. B. Martonen, "Flow transition in bends and applications to airways", *J. Aero. Sci.,* vol. 31**,** pp. 831-847, 2000.

[11] P. Mishra, and S. N. Gupta, "Momentum transfer in curved pipes", 2. Non-Newtonian fluids, *Ind. Eng. Chem. Process Dev*., vol. 18(1), pp. 137-142, 1979.

[12] Fluent user guide USA, 2007.